MATERIALS CHEMISTRY FRONTIERS

CHINESE CHEMICAL SOCIETY

ROYAL SOCIETY OF CHEMISTRY

RESEARCH ARTICLE

View Article Online
View Journal | View Issue

Cite this: *Mater. Chem. Front.*, 2020, **4**, 1671

Spatially separated bimetallic cocatalysts on hollow-structured TiO_2 for photocatalytic hydrogen generation†

Ping She, [a] Jun-sheng Qin, [ab] Heng Rao, [ab] Buyuan Guan[ab] and Jihong Yu *[ab]

Received 25th January 2020,
Accepted 24th March 2020

DOI: 10.1039/d0qm00042f

rsc.li/frontiers-materials

Efficient charge separation and light harvesting of photocatalysts (*e.g.*, TiO_2) are the key issues to be considered in the design of solar-energy conversion systems. In particular, the charge separation of noble metal-decorated TiO_2 materials could be greatly improved *via* decreasing the size of noble metal particles (NPs). Furthermore, designing specific morphologies such as hollow structures can improve light harvesting ability. Herein, a hybrid hollow TiO_2 with spatially separated bimetals (Pd@TiO_2@Au) was prepared, which demonstrated enhanced charge separation. By choosing zeolite as the sacrificial substrate, ultrasmall Pd NPs and Au NPs were decorated in the inner and outer shells of hollow TiO_2, respectively. The separated bimetals could pull the photoexcited electrons away from the surface of TiO_2 for more efficient charge separation. The as-prepared Pd@TiO_2@Au catalyst exhibited a superior photocatalytic H_2 evolution rate up to 272.3 μmol h^{-1}, which was higher than most of the TiO_2-based photocatalysts.

Introduction

Nowadays, the problem of energy shortage and environmental pollution is becoming more and more serious in the world.[1–5] Hydrogen (H_2) as a kind of clean fuel has drawn intensive attention for its superior energy density and environmental friendliness.[1–3] Converting solar energy into H_2 by photocatalytic water splitting is one of the most efficient ways for H_2 production. A large number of semiconductor photocatalysts including titanium dioxide (TiO_2), CdS, Ta_3N_5, ZnO and g-C_3N_4 have been widely used for photocatalytic H_2 generation.[6,7] Among them, TiO_2 has been considered as one of the most promising photocatalysts owing to its low price, high safety and superior chemical stability.[8–11] However, the fast recombination of the photogenerated electron–hole pairs strongly hinders the photocatalytic hydrogen production. Recently, noble metal nanoparticles (NPs) (*e.g.*, Au, Pt, and Ag NPs) were decorated on photocatalysts to enhance the catalytic properties.[12–15] In particular, the bimetal decorated TiO_2 (such as Pd–Au, Pt–Cu, and Au–Pt) can exhibit further improved photocatalytic efficiency compared to the monometal decorated ones.[16–20] Among them, most of the bimetals were randomly decorated outside the TiO_2 with the inner interface not being used. Thus, the spatially separated bimetals on the inner and outer surfaces of TiO_2 are expected to be able to enhance the photocatalytic properties by fully utilizing the photo-induced charges on the interface of excited TiO_2.

On the other hand, recent investigations showed that the size of noble metal NPs has a great influence on the photocatalytic properties of the nanohybrids.[6,21] It has been demonstrated that the smaller noble metal NPs can induce a lower Fermi level, which can cause improved charge transfer and an elevated separation rate of electron–hole pairs.[21] Unfortunately, it is hard to obtain ultrasmall noble metal clusters since they are prone to aggregation. Nowadays, zeolites have been widely used for the confinement synthesis of ultrasmall metal NPs and even sub-nanometric metallic clusters, in which the nanospace of zeolites can restrict the growth of the metals.[22–24] Also, the ordered microporous structures of zeolites can eliminate the aggregation of metal species and thus improve the catalytic properties and stability.[25]

Furthermore, it has been demonstrated that the nanostructures of the hybrids of noble metal–TiO_2 play an important role in improving the photocatalytic properties.[11,26–30] Notably, the nano hybrids with a yolk–shelled hollow morphology can induce higher photocatalytic properties.[30] On the one hand, the hollow structure can enhance light utilization efficiency by realizing repeated light reflection and refraction; on the other hand, the hollow structure can increase the surface-to-volume ratio,

[a] *State Key Laboratory of Inorganic Synthesis and Preparative Chemistry, College of Chemistry, Jilin University, 2699 Qianjin Street, Changchun 130012, P. R. China. E-mail: jihong@jlu.edu.cn*

[b] *International Center of Future Science, Jilin University, 2699 Qianjin Street, Changchun 130012, P. R. China*

† Electronic supplementary information (ESI) available: Additional characterization results including SEM images, TEM images, EDS mapping images, XRD patterns, and time courses of photocatalytic H_2 evolution. See DOI: 10.1039/d0qm00042f

which can provide more active reaction sites and enhance mass transfer.

Herein, we designed a hollow-structured TiO_2 with spatially separated bimetallic NPs decorated in the core and outer shells, respectively. In detail, the hollow TiO_2 sphere was obtained by choosing silicalite-1 (MFI) zeolite with embedded ultrasmall Pd NPs as a supporting substrate followed by etching of the zeolite. The TiO_2 exhibited a hollow structure and the ultrasmall Pd NPs were decorated inside the hollow TiO_2 sphere. Then, Au NPs working as the cocatalyst were decorated on the outer surfaces of the TiO_2 shell. The obtained sandwich-like hollow-structured Pd@TiO_2@Au with spatially separated cocatalysts can significantly enhance the photocatalytic properties of TiO_2 by combining the surface plasmon resonance (SPR) effect of Au NPs and the smaller size effect of Pd NPs. Specifically, Pd@TiO_2@Au exhibited a superior photocatalytic H_2 evolution rate up to 272.3 μmol h^{-1}. Such performance is far superior to most of the TiO_2-based photocatalysts for water-splitting.

Experimental

Materials

Chloroauric acid tetrahydrate ($HAuCl_4{\cdot}4H_2O$, A.R., Shanghai Chemical Factory), tetraethylorthosilicate (TEOS) (Sinopharm Chemical Reagent Co., Ltd), tetrabutyl orthotitanate (TBOT) (98%, Macklin), tetrapropylammonium hydroxide (TPAOH) (25 wt%, Tianjin Guangfu Fine Chemical Research Institute), ethanol (99%, Tianjin Guangfu Fine Chemical Research Institute), palladium chloride ($PdCl_2$, Pd 59%, Aladdin), ethylenediamine ($NH_2CH_2CH_2NH_2$, Tianjin Fuchen Chemical Reagents Factory), ammonia ($NH_3{\cdot}H_2O$, Tianjin Yongsheng Fine Chemical Co., Ltd), sodium hydroxide (NaOH, A.R., Tianjin Yongsheng Fine Chemical Co., Ltd), and deionized water (resistance >18 MΩ cm^{-1}).

Preparation of silicalite-1 (S1) zeolite

S1 was prepared by using the hydrothermal method at 170 °C for 4 days, the molar composition of which is $1.0SiO_2 : 0.4$ TPAOH : $35H_2O$. Specifically, 13 g of TPAOH was mixed with deionized water followed by stirring for 10 min, then 8.32 g of TEOS was added to the above solution. After being stirred for 6 h, the mixture was transferred to a Teflon-lined stainless-steel autoclave and heated at 170 °C for 4 days under static conditions. After washing with deionized water and ethanol three times, the product was then dried at 60 °C. Finally, conventional S1 was obtained by calcinating the above product at 550 °C in air for 8 h.

Synthesis of Pd@silicalite-1 (Pd@S1)

Pd@S1 was synthesized using the same method for the preparation of S1 except for the addition of $[Pd(NH_2CH_2CH_2NH_2)_2]Cl_2$ after the hydrolysis of TEOS.[27] After calcination, the product was subsequently reduced with H_2 at 400 °C for 2 h. In this way, Pd@S1 was obtained.

Preparation of hollow Pd@TiO_2, hollow TiO_2 and TiO_2 NPs

Typically, 150 mg of the above-synthesized zeolite or Pd@S1 was dispersed in 200 mL of absolute ethanol. After adding 0.9 mL of ammonia solution (28 wt%) into the system followed by ultrasonication for half an hour, TBOT (2.0 mL) was added into the solution drop by drop. Then, the mixture was stirred at 45 °C for 24 hours. After washing with deionized water and ethanol several times and calcination at 450 °C for 2 h, Pd@S1@TiO_2 NPs were obtained. In order to get hollow structured Pd@TiO_2, 50 mg of Pd@S1@TiO_2 NPs was treated with 30 mL of NaOH solution (3 M) under stirring for 12 h. After centrifugation and washing with water and ethanol 3 times, hollow Pd@TiO_2 was obtained. When it comes to the synthesis of hollow TiO_2 NPs, S1 was used to replace Pd@S1. The conventional TiO_2 NPs were prepared using the same method for preparing hollow TiO_2 except without adding zeolite as the template.

Preparation of sandwich-like Pd@TiO_2@Au, hollow TiO_2@Au, Pd@TiO_2@Pt and hollow TiO_2@Pt

The sandwich-like Pd@TiO_2@Au was synthesized by photo-deposition of the Au NPs on the surfaces of Pd@TiO_2. Specifically, the starting gel of sandwich-like Pd@TiO_2@Au was obtained by dispersing Pd@TiO_2 into $HAuCl_4$ (0.06%) solution and adjusting the pH to 8 (adjusted by 0.1 M NaOH). After irradiation at 200–1100 nm for 20 minutes, Au^{3+} was converted into Au NPs. In this way, the sandwich-like Pd@TiO_2@Au was obtained. The hollow TiO_2@Au was obtained by replacing Pd@TiO_2 with hollow TiO_2. The sandwich-like Pd@TiO_2@Pt was synthesized using the same method except for replacing $HAuCl_4$ by H_2PtCl_6. The hollow TiO_2@Pt was prepared by replacing Pd@TiO_2 with hollow TiO_2.

Synthesis of Pd-im/silicalite-1 (Pd-im/S1) and Pd-im@TiO_2

For comparison, Pd-im/S1 was obtained using the impregnation method.[27] Typically, 0.23 mL of $(NH_4)_2PdCl_4$ solution (0.28 M) was added into 1 g of S1. After stirring for an hour, the mixture was dried overnight at 80 °C. Finally, Pd-im/S1 was obtained by reducing the dried mixture with hydrogen. Then, Pd-im@TiO_2 was prepared using the same method for preparing Pd@TiO_2 except for replacing Pd@S1 by Pd-im/S1.

Synthesis of Pd–Au-im@TiO_2 and Pd–Pt-im@TiO_2

Pd–Au-im@TiO_2 and Pd–Pt-im@TiO_2 were prepared using the impregnation approach. The metal loadings in Pd–Au-im@TiO_2 and Pd–Pt-im@TiO_2 were controlled to be comparable with those of sandwich-like Pd@TiO_2@Au and Pd@TiO_2@Pt accordingly. First, Pd@S1 was impregnated with $HAuCl_4$ and H_2PtCl_6 solutions, respectively. Then, Pd–Au-im@S1 and Pd–Pt-im@S1 were obtained by reducing the above two mixtures with hydrogen at 400 °C for 2 h. Finally, Pd–Au-im@TiO_2 and Pd–Pt-im@TiO_2 were obtained by growing TiO_2 on the outside surface of Pd–Au-im@S1 and Pd–Pt-im@S1, respectively, followed by etching the zeolite with NaOH solution. The methods for the growth of TiO_2 and the etching details are the same as those for the preparation of sandwich-like Pd@TiO_2@Au.

Material characterization

Powder X-ray diffraction was performed on a Rigaku Smart Lab X-ray diffractometer using Cu Kα radiation (λ = 1.5418 Å) in the 2θ range from 4° to 80°. Scanning electron microscopy (SEM)

images and energy dispersive X-ray (EDX) spectrometry images were obtained using a JSM-7800F (Japan) electron microscope. The transmission electron microscopy (TEM) images and EDX spectrometry images were obtained using a Tecnai F20 electron microscope. The metal loading was determined using inductively coupled plasma (ICP) analyses on a PerkinElmer Optima 3300 DV ICP instrument. X-ray photoelectron spectroscopy (XPS) was carried out on an ESCALAB 250 spectrometer. UV-vis absorption spectra were obtained using a SHIMADZU UV-2550 spectrophotometer (200–800 nm). The photoluminescence (PL) spectral measurements were conducted on a SHIMADZU RF-5301pc spectrofluorophotometer. The PL lifetime decay curves were plotted using a HORIBA Scientific FluoroMax-4 spectrofluorometer.

Photocatalytic measurements

Typically, 10 mg of the photocatalyst was dispersed in 20 mL of an aqueous solution containing 4 mL of methanol, then the solution was transferred into a quartz vessel. After being vacuumed for 20 min to remove the dissolved air, the vessel was irradiated by a 300 W Xenon lamp under simulated solar light (200–1100 nm) with a light intensity of 250 mW cm^{-2}. The gas products generated from photocatalytic water splitting were analyzed periodically using an Agilent 7890A gas chromatograph (GC) with a thermal conductivity detector (TCD).

Photocurrent measurements

The electrochemical experiments were performed on a CHI 660E electrochemistry work station in Na_2SO_4 (0.5 M) solution. Platinum wire and the AgCl/Ag electrode (saturated with KCl) were used as the counter electrode and the reference electrode, respectively. The working electrodes were made by loading the samples on indium-tin oxide (ITO). In detail, 10 mg of the photocatalysts was dispersed in 200 μL of deionized water, and then the obtained slurry was dropped onto ITO to form a square with the area of 1 cm^2 followed by drying at 50 °C for 30 min. Following dropping 20 μL of Nafion on the surface of the photocatalysts, the photoelectrodes of hollow TiO_2, hollow TiO_2@Pt, Pd@TiO_2 and Pd@TiO_2@Au were obtained. Light illumination was provided by a 300 W Xe lamp with the light intensity of 300 mW cm^{-2}.

Results and discussion

The synthesis process of the sandwich-like hollow-structured Pd@TiO_2@Au photocatalyst is shown in Fig. 1. First, ultrasmall Pd NPs were obtained by using an MFI type zeolite (silicalite-1) as the host matrix and $[Pd(NH_2CH_2CH_2NH_2)_2]Cl_2$ as the metal precursor, respectively, using the method developed by our group.[31] Specifically, the precursor of Pd NPs was introduced to the hydrothermal crystallization process of silicalite-1 (S-1). After calcination and followed by reduction with H_2, the ultrasmall Pd NPs confined in silicalite 1 (Pd@S1) were obtained. Subsequently, Pd@S1 was covered with a layer of amorphous TiO_2 after mixing Pd@S1 in tetrabutyl titanate (TBOT) and ammonia solution at 45 °C for 24 h. Following calcination at 450 °C for 2 h, Pd@S1@TiO_2 with anatase TiO_2 was obtained.

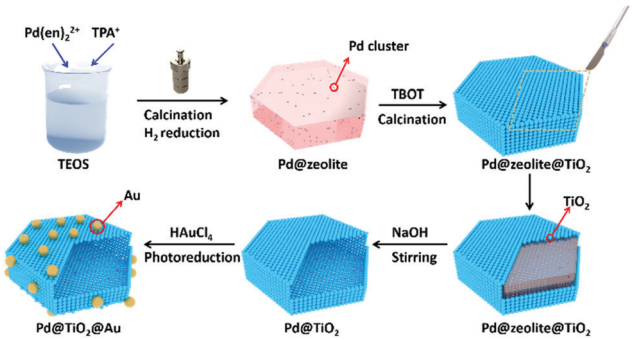

Fig. 1 Schematic illustration for the preparation of the sandwich-like Pd@TiO_2@Au photocatalyst.

Afterwards, Pd@S1@TiO_2 was transformed into hollow-structured Pd@TiO_2 after being treated with the NaOH solution. In this way, the sandwich-like hollow-structured Pd@TiO_2@Au was achieved by photo-reducing $HAuCl_4$ on the outer surface of Pd@TiO_2. For comparison, hollow TiO_2 and conventional TiO_2 NPs were also prepared by using pure S1 as the sacrificial substrate and without adding zeolites, respectively. In addition, Pd-im@TiO_2 with larger Pd NPs was achieved by growing TiO_2 on the outside surface of Pd-im/S1 (obtained using the impregnation method). In order to further elucidate the effect of spatially separated cocatalysts on the sandwich-like hollow structured Pd@TiO_2@Au photocatalyst, Pd–Au-im@TiO_2 with both the cocatalysts (Pd and Au NPs) decorated on the inner surface of hollow TiO_2 was prepared.

As shown in the scanning electron microscopy (SEM) and transmission electron microscopy (TEM) images (Fig. 2 and Fig. S1, S2, ESI†), S1, Pd@S1, Pd@TiO_2 and the sandwich-like Pd@TiO_2@Au all display the shape of a hexagonal prism with the size of about 200–300 nm. According to the TEM images of Pd@S1 obtained

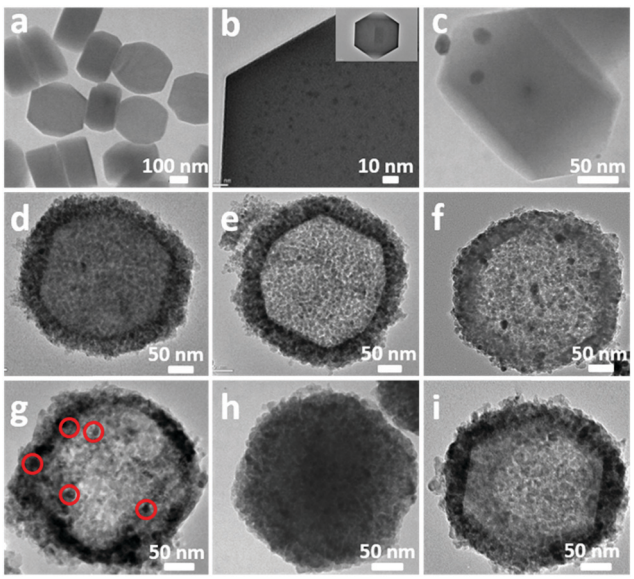

Fig. 2 TEM image of Pd@S1 in lower (a) and higher magnification (b); (c) TEM image of Pd-im/S1; (d) TEM image of Pd@S1@TiO_2; (e) TEM image of Pd@TiO_2; (f) TEM image of Pd@TiO_2@Au; (g) TEM image of Pd-im@TiO_2; (h) TEM image of S1@TiO_2; (i) TEM image of hollow TiO_2.

by the *in situ* process, the ultrasmall Pd clusters (<2 nm) are uniformly located inside the zeolite crystals (Fig. 2a and b). In comparison, the Pd-im/S1 sample prepared by the impregnation method possesses a larger size of Pd NPs (~10 nm), as shown in Fig. 2c. The TEM image of Pd@S1@TiO_2 in Fig. 2d shows that a layer of TiO_2 with the thickness of about 35 nm covers the outer surface of Pd@S1. As shown in Fig. 2e and f, both Pd@TiO_2 and Pd@TiO_2@Au exhibit a hollow structure. Due to the small size, the inner Pd NPs are invisible. The Au NPs in Pd@TiO_2@Au decorated on the outer surface of hollow Pd@TiO_2 are about 10 nm in size. In contrast, the Pd NPs in the hollow Pd-im@TiO_2 (Fig. 2g) are more obvious for their larger size. In addition, the hexagonal S1@TiO_2 (Fig. 2h) and hollow TiO_2 (Fig. 2i) and conventional TiO_2 NPs (Fig. S3, ESI†) were also obtained.

The SEM and TEM elemental mappings of Pd@TiO_2 and Pd@TiO_2@Au are shown in Fig. 3a–i and Fig. S4 (ESI†), revealing the existence of Pd, Ti, O and Au elements. The Pd, Ti and O elements are distributed uniformly in hollow-structured Pd@TiO_2 and Pd@TiO_2@Au. Furthermore, it appears that the Au NPs are deposited on the outside surface of hollow TiO_2 in sandwich-like Pd@TiO_2@Au (Fig. S4, ESI†). According to the inductively coupled plasma atomic emission spectroscopy (ICP-AES) analysis, the Au and Pd loading in the sandwich-like hollow-structured Pd@TiO_2@Au is 4.89 and 0.62 wt%, respectively.

The as-prepared sandwich-like hollow-structured Pd@TiO_2@Au photocatalyst was further characterized using X-ray diffraction (XRD). The as-synthesized S1 and Pd@S1 exhibit the typical diffraction peaks of the MFI zeolite structure (Fig. S5, ESI†).[22] For Pd@S1@TiO_2, the diffraction peaks belonging to anatase-TiO_2 can be obviously seen (Fig. S6, ESI†).[29] According to Fig. S6, S7 (ESI†) and Fig. 4a, all the TiO_2-containing samples (TiO_2 NPs, hollow TiO_2, Pd@TiO_2, hollow TiO_2@Au and Pd@TiO_2@Au) show typical diffraction peaks of anatase-TiO_2. Besides, the peaks of face-centered-cubic Au can be seen in the XRD profiles of hollow TiO_2@Au and Pd@TiO_2@Au.[29]

The UV-vis spectra in Fig. 4b indicate that the existence of both Pd NPs and Au NPs can enhance the light absorption of hollow TiO_2. Furthermore, Pd@TiO_2@Au with spatially separated Pd NPs and Au NPs exhibits much higher light absorption efficiency than the hollow TiO_2 and monometal cocatalyst decorated ones (Pd@TiO_2 and hollow TiO_2@Au). Besides, TiO_2@Au and Pd@TiO_2@Au with decorated Au NPs show much higher light absorption ability in the visible light range, which may be caused by the elevated light absorption due to the SPR effect and the light scattering of Au NPs.[27]

The X-ray photoelectron spectroscopy (XPS) analyses of sandwich-like Pd@TiO_2@Au are shown in Fig. 4c–f. There are two peaks belonging to Ti 2p that appear at around 458.8 and 464.7 eV, indicating the Ti^{4+} valence state in octahedral coordination with oxygen.[32] The signal of O 1s exhibits a peak at 530.2 eV corresponding to the Ti–O bonds in the TiO_2 lattice, and the peak located at the shoulder (532.4 eV) is related to the oxygen in the surface hydroxyl groups.[33] The peak at 335.1 attributed to Pd $3d_{5/2}$ is observed in Pd@TiO_2@Au, which is related to the zero-valent Pd NPs.[31] The Au 4f spectrum displays two peaks at 83.3 and 87.0 eV with the splitting of 3.7 eV, indicating the metallic nature of Au.[34]

The photocatalytic H_2 evolution activities of sandwich-like Pd@TiO_2@Au together with hollow TiO_2, Pd@TiO_2, and hollow TiO_2@Au were investigated under simulated solar light. In the photocatalytic reaction system, methanol (CH_3OH) was added as the sacrificial agent to react with the holes. As shown in Fig. 5a–b and Fig. S8 (ESI†), all of the hollow-structured photocatalysts exhibit enhanced hydrogen generation compared to the TiO_2 NPs. The H_2 evolution rate of hollow TiO_2 (14.3 μmol h^{-1}) is about 2 times faster than that of the TiO_2 NPs (6.5 μmol h^{-1} in Fig. S8, ESI†). This phenomenon can be attributed to the elevated light harvesting induced by the hollow structure. Notably, Pd@TiO_2@Au with spatially separated bimetallic cocatalysts shows greatly improved photocatalytic properties. The H_2 generation rate of Pd@TiO_2 and TiO_2@Au reaches up to 210.8 and 119.5 μmol h^{-1}, respectively. Significantly, Pd@TiO_2@Au gives a H_2 generation rate up to 272.3 μmol h^{-1}. For comparison, we also prepared sandwich-like Pd@TiO_2@Pt by using Pt to replace Au to further test whether different separated bimetallic cocatalysts on TiO_2 could still work (Fig. 5c). The morphologies of Pd@TiO_2@Pt, hollow TiO_2@Pt and Pt-im/Pd@S1 are shown in Fig. S9 and S10 (ESI†). As expected, Pd@TiO_2@Pt with similar types of spatially separated cocatalysts (Pd NPs and Pt NPs) shows an enhanced hydrogen evolution rate (648.6 μmol h^{-1}) compared to TiO_2 NPs and hollow TiO_2. In addition, Pd@TiO_2@Pt gives a higher elevated hydrogen evolution rate than Pd@TiO_2 (210.8 μmol h^{-1}) and TiO_2@Pt (464.0 μmol h^{-1}). To further

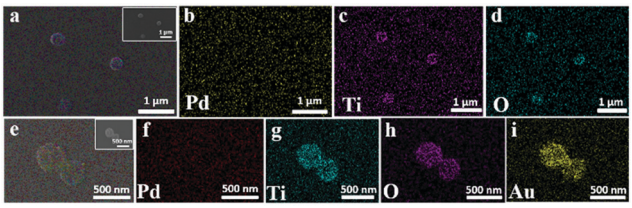

Fig. 3 Elemental mapping images of Pd@TiO_2 (a)–(d) and sandwich-like Pd@TiO_2@Au (e)–(i): (a and e) the corresponding overlapped elemental mapping images of Pd, Ti, and O and Pd, Ti, O and Au respectively, and the insets in (a) and (e) are the corresponding SEM images; (b and f) Pd mapping images; (c and g) Ti mapping images; (d and h) O mapping images; and (i) Au mapping image.

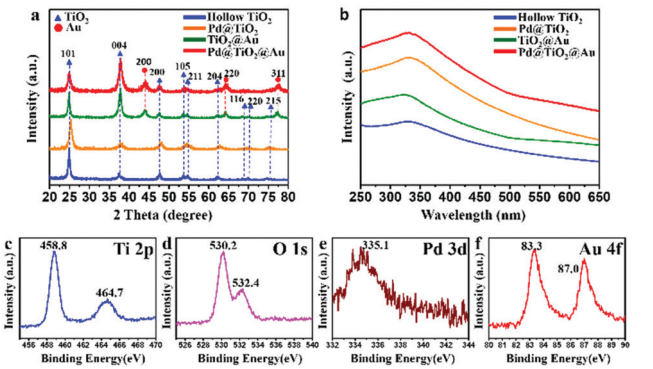

Fig. 4 (a) XRD profiles and UV-vis spectra (b) of hollow TiO_2, Pd@TiO_2, hollow TiO_2@Au and sandwich-like Pd@TiO_2@Au; (c)–(f) XPS spectra of sandwich-like Pd@TiO_2@Au.

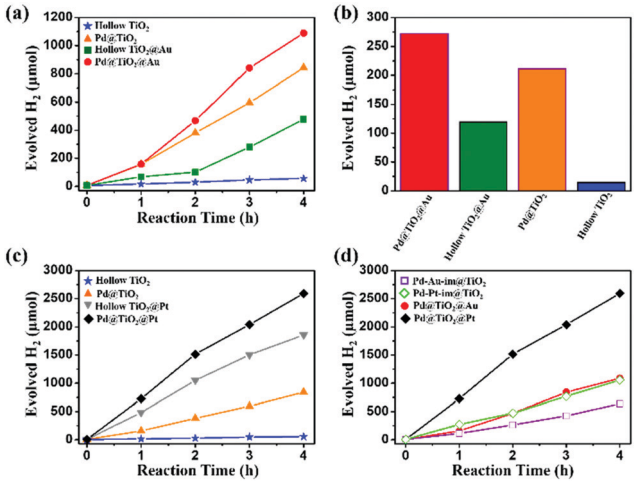

Fig. 5 (a) H_2 generation over the sandwich-like Pd@TiO_2@Au catalyst, hollow TiO_2, Pd@TiO_2 and hollow TiO_2@Au; (b) H_2 evolution rates based on the corresponding catalysts in Fig. 5a; (c) H_2 generation over the Pd@TiO_2@Pt catalyst and the corresponding controls; (d) H_2 generation over Pd–Au-im@TiO_2 and Pd–Pt-im@TiO_2 for comparison with Pd@TiO_2@Au and Pd@TiO_2@Pt.

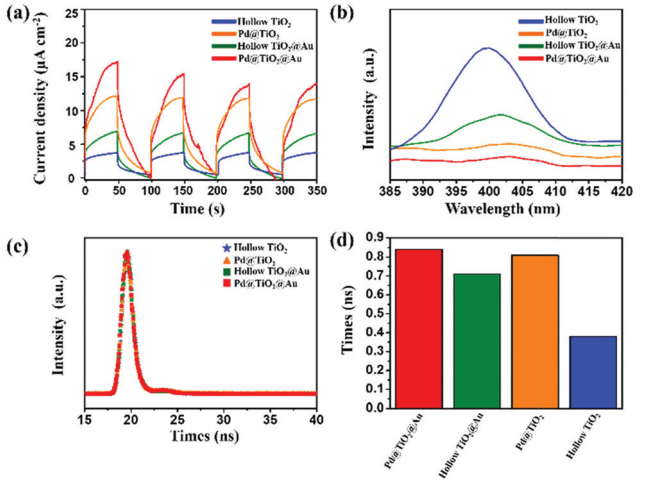

Fig. 6 Photocurrent generation performance (a), PL spectra (b), PL lifetime decay curves (c) and the bar chart of PL decay time (d) of hollow TiO_2, Pd@TiO_2, hollow TiO_2@Au and sandwich-like Pd@TiO_2@Au.

demonstrate the effects of the spatially separated cocatalysts on TiO_2, Pd–Au-im@TiO_2 and Pd–Pt-im@TiO_2 with both bi-noble metal NPs decorated within the hollow cavity were also prepared to compare with Pd@TiO_2@Au and Pd@TiO_2@Pt correspondingly (Fig. 5d). The H_2 generation rates of Pd–Au-im@TiO_2 and Pd–Pt-im@TiO_2 are 159.3 and 264.2 μmol h^{-1}, respectively, which are much lower than that of Pd@TiO_2@Au and Pd@TiO_2@Pt decorated with the spatially separated bimetallic cocatalyst. Therefore, we can conclude that spatially separated bi-noble metals play an important role in enhancing the photocatalytic efficiency.

On the other hand, the size effect of Pd NPs plays an important role in the photocatalytic efficiency of Pd@TiO_2. For comparison, Pd-im@TiO_2 with larger sized Pd NPs was also obtained by replacing Pd@S1 with Pd-im/S1 to work as the sacrificial substrate. As shown in Fig. S11 (ESI†), Pd-im@TiO_2 shows a lower hydrogen evolution rate (163.5 μmol h^{-1}) than Pd@TiO_2 (210.8 μmol h^{-1}). Therefore, the smaller sized Pd NPs synthesized by *in situ* crystallization of the zeolite can further improve the catalytic properties of TiO_2. It is worth mentioning that the hydrogen generation rate of sandwich-like Pd@TiO_2@Au (272.3 μmol h^{-1}) with the quantum efficiency of 1.64% (Fig. S12, ESI†) is superior to most of the TiO_2-based photocatalysts for photocatalytic hydrogen generation under similar conditions (Table S1, ESI†).[34–42]

Fig. 6a shows the photocurrent generation performance of hollow TiO_2, Pd@TiO_2, hollow TiO_2@Au and sandwich-like Pd@TiO_2@Au. It can be clearly seen that the existence of Pd NPs and Au NPs can improve the photocurrent density. Specifically, the sandwich-like Pd@TiO_2@Au with spatially separated cocatalysts exhibits the highest photocurrent density, demonstrating the efficient photoinduced charge separation properties. To further investigate the charge separation properties of the as-prepared photocatalysts, the photoluminescence (PL) emission spectrum was recorded. As shown in Fig. 6b, all the samples exhibit characteristic peaks at around 400 nm. In detail, all the TiO_2 hybrids with decorated cocatalysts (Pd NPs or Au NPs) show weaker PL emission compared to hollow TiO_2, which may be attributed to the lower Fermi level of Pd NPs and Au NPs.[21] Furthermore, the PL emission of Pd@TiO_2 is lower than that of hollow TiO_2@Au, suggesting that Pd@TiO_2 possesses greater charge transfer ability than hollow TiO_2@Au. Notably, the sandwich-like Pd@TiO_2@Au exhibits the weakest PL emission among all of the samples, further confirming the superior charge separation performance. To better understand the behaviour of the photo-excited charge carriers, the time-resolved fluorescence decay spectra of the as-prepared photocatalysts were also studied (Fig. 6c). According to the bar chart of PL decay time shown in Fig. 6d, the sandwich-like Pd@TiO_2@Au displays a longer decay time than the other samples, further indicating the superior charge separation of the photocatalyst with spatially separated bimetals.

The proposed mechanism of photocatalytic hydrogen generation over the sandwich-like Pd@TiO_2@Au catalyst is shown in Fig. 7. Upon irradiation by incident light, holes are generated

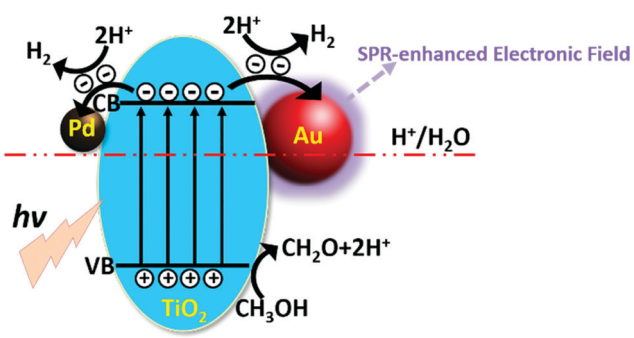

Fig. 7 Proposed mechanism of photocatalytic hydrogen generation over the Pd@TiO_2@Au catalyst.

on the valence band (VB) of TiO_2 and photo-induced electrons are produced on the conduction band (CB). Subsequently, the photo-induced electrons can be quickly transferred from TiO_2 to the cocatalysts (Pd NPs and Au NPs).[43,44] In addition, the SPR effect induced by the Au NPs on the outside surface of TiO_2 can stimulate an enhanced electronic field, which can not only improve the generation rate of electron–hole pairs, but also facilitate the charge transfer.[45] Meanwhile, charge separation can be further improved by the ultrasmall size effect of Pd NPs located on the inner surface of TiO_2.[46] In this way, more efficient charge transfer and quantum efficiency can be obtained. Moreover, the photo-generated holes on the VB of TiO_2 can be used to oxidize the scavenger (CH_3OH) to produce H^+ ions. Afterward, the H^+ ions can combine with the electrons on the CB of TiO_2 or cocatalysts to produce H_2. Specifically, the spatially separated bimetallic cocatalysts can further enhance the photocatalytic properties of sandwich-like Pd@TiO_2@Au due to the enhanced charge separation, as shown in Fig. 6.

Conclusions

A hollow-structured TiO_2 decorated with spatially separated bimetallic cocatalysts (Pd@TiO_2@Au) was obtained by using a zeolite as the sacrificial substrate. Pd@TiO_2@Au exhibits superior photocatalytic hydrogen generation ability based on the factors below: first, the hollow structure of TiO_2 can not only enhance light utilizing ability by repeated light reflection and refraction, but also provide more active reaction sites and facilitate mass transfer through the enhanced specific surface area. Second, the spatially separated bimetallic cocatalysts (Pd and Au) can further increase the photocatalytic charge transfer and separation by fully utilizing the photo-induced charges on both the inner and outer surfaces of the excited TiO_2. Thirdly, the SPR effect induced by the Au NPs on the outside surface of TiO_2 can stimulate an enhanced electronic field, which can not only improve the generation rate of electron–hole pairs, but also facilitate the charge transfer. Fourth, the ultra-small Pd NPs synthesized by the *in situ* crystallization process of zeolite can further elevate the charge separation efficiency. The facile approach demonstrated here holds great promise for the design of highly efficient photocatalysts for the application of environmental purification and solar-to-hydrogen energy conversion.

Conflicts of interest

There are no conflicts to declare.

Acknowledgements

We gratefully acknowledge the National Key Research and Development Program of China (Grant 2016YFB0701100), the National Natural Science Foundation of China (Grant 21835002 and 21621001), the 111 Project (B17020), the Post Doctoral Innovative Talent Support Program (BX20180122) and the China Postdoctoral Science Foundation (2019M651195) for supporting this work.

Notes and references

1 J. L. Wu, Z. Y. Zhang, B. K. Liu, Y. R. Fang, L. Wang and B. Dong, UV-Vis-NIR-driven plasmonic photocatalysts with dual-resonance modes for synergistically enhancing H_2 generation, *Sol. RRL*, 2018, **2**, 1800039.

2 Y. Liu, Z. Y. Zhang, Y. R. Fang, B. K. Liu, J. D. Huang, F. J. Miao, Y. A. Bao and B. Dong, IR-driven strong plasmonic-coupling on Ag nanorices/$W_{18}O_{49}$ nanowires heterostructures for photo/thermal synergistic enhancement of H_2 evolution from ammonia borane, *Appl. Catal., B*, 2019, **252**, 164–173.

3 D. P. Dong, C. X. Yan, J. D. Huang, N. Lu, P. Y. Wu, J. Wang and Z. Y. Zhang, An electron-donating strategy to guide the construction of MOF photocatalysts toward co-catalyst-free highly efficient photocatalytic H_2 evolution, *J. Mater. Chem. A*, 2019, **7**, 24180–24185.

4 M. Y. Zhang, Y. Qi and Z. Y. Zhang, AgBr/BiOBr nano-heterostructure-decorated polyacrylonitrile nanofibers: a recyclable high-performance photocatalyst for dye degradation under vsible-light irradiation, *Polymers*, 2019, **11**, 1718.

5 P. Zhang, D. Y. Wan, Z. Y. Zhang, G. D. Wang, J. H. Hu and G. S. Shao, RGO-functionalized polymer nanofibrous membrane with exceptional surface activity and ultra-low airflow resistance for PM2.5 filtration, *Environ. Sci.: Nano*, 2018, **5**, 1813–1820.

6 Q. M. Sun, N. Wang, J. H. Yu and J. C. Yu, A hollow porous CdS photocatalyst, *Adv. Mater.*, 2018, **30**, 1804368.

7 Y. G. Zhu, Z. Y. Zhang, N. Lu, R. N. Hua and B. Dong, Prolonging charge-separation states by doping lanthanide-ions into {001}/{101} facets-coexposed TiO_2 nanosheets for enhancing pho-cmssmark tocatalytic H_2 evolution, *Chin. J. Catal.*, 2019, **40**, 413–423.

8 C. Tang, L. F. Liu, Y. L. Li and Z. F. Bian, Aerosol spray assisted assembly of TiO_2 mesocrystals into hierarchical hollow microspheres with enhanced photocatalytic performance, *Appl. Catal., B*, 2017, **201**, 41–47.

9 M. Z. Ge, Q. S. Li, C. Y. Cao, J. Y. Huang, S. H. Li, S. N. Zhang, Z. Chen, K. Q. Zhang, S. S. Al-Deyab and Y. K. Lai, One-dimensional TiO_2 nanotube photocatalysts for solar water splitting, *Adv. Sci.*, 2017, **4**, 1600152.

10 Y. X. Zhao, Y. F. Zhao, R. Shi, B. Wang, G. I. N. Waterhouse, L. Z. Wu, C. H. Tung and T. R. Zhang, Tuning oxygen vacancies in ultrathin TiO_2 nanosheets to boost photocatalytic nitrogen fixation up to 700 nm, *Adv. Mater.*, 2019, **31**, 1806482.

11 Z. W. Seh, S. H. Liu, M. Low, S. Y. Zhang, Z. L. Liu, A. Mlayah and M. Y. Han, Janus Au–TiO_2 photocatalysts with strong localization of plasmonic near-fields for efficient visible-light hydrogen generation, *Adv. Mater.*, 2012, **24**, 2310–2314.

12 Z. Q. Liang, Y. C. Guo, Y. J. Xue, H. Z. Cui and J. Tian, 1T-phase MoS_2 quantum dots as a superior co-catalyst to Pt decorated on carbon nitride nanorods for photocatalytic hydrogen evolution from water, *Mater. Chem. Front.*, 2019, **3**, 2032–2040.

13 J. L. He, S. Li, D. Lyu, D. F. Zhang, X. Wu and Q. H. Xu, Aggregation induced emission enhancement by plasmon coupling of noble metal nanoparticles, *Mater. Chem. Front.*, 2019, **3**, 2421–2427.

14 L. Cheng, D. N. Zhang, Y. L. Liao, F. Li, H. W. Zhang and Q. J. Xiang, Constructing functionalized plasmonic gold/titanium dioxide nanosheets with small gold nanoparticles for efficient photocatalytic hydrogen evolution, *J. Colloid Interface Sci.*, 2019, **555**, 94–103.

15 S. Q. Kong, X. M. Song, C. W. Zhang, W. Wang and G. C. Yan, Photocatalytic activity and photodegradation rate constant of Au–TiO_2 nanofilms by magnetron sputtering, *Rare Met. Mater. Eng.*, 2018, **47**, 3316–3320.

16 Z. Y. Zhang, S. W. Cao, Y. S. Liao and C. Xue, Selective photocatalytic decomposition of formic acid over AuPd nanoparticle-decorated TiO_2 nanofibers toward high-yield hydrogen production, *Appl. Catal., B*, 2015, **162**, 204–209.

17 Z. Y. Zhang, A. R. Li, S. W. Cao, M. Bosman, S. Z. Li and C. Xue, Direct evidence of plasmon enhancement on photocatalytic hydrogen generation over Au/Pt-decorated TiO_2 nanofibers, *Nanoscale*, 2014, **6**, 5217–5222.

18 H. B. Yu, X. H. Wang, H. W. Sun and M. X. Huo, Photocatalytic degradation of malathion in aqueous solution using an Au–Pd–TiO_2 nanotube film, *J. Hazard. Mater.*, 2010, **184**, 753–758.

19 Y. Shiraishi, H. Sakamoto, Y. Sugano, S. Ichikawa and T. Hirai, Pt-Cu bimetallic alloy nanoparticles supported on anatase TiO_2: highly active catalysts for aerobic oxidation driven by visible light, *ACS Nano*, 2013, **7**, 9287–9297.

20 A. Gallo, M. Marelli, R. Psaro, V. Gombac, T. Montini, P. Fornasiero, R. Pievo and V. Dal Santo, Bimetallic Au–Pt/TiO_2 photocatalysts active under UV-A and simulated sunlight for H_2 production from ethanol, *Green Chem.*, 2012, **14**, 330–333.

21 K. Qian, B. C. Sweeny, A. C. Johnston-Peck, W. X. Niu, J. O. Graham, J. S. DuChene, J. J. Qiu, Y. C. Wang, M. H. Engelhard, D. Su, E. A. Stach and W. D. Wei, Surface plasmon-driven water reduction: gold nanoparticle size matters, *J. Am. Chem. Soc.*, 2014, **136**, 9842–9845.

22 T. L. Cui, W. Y. Ke, W. B. Zhang, H. H. Wang, X. H. Li and J. S. Chen, Encapsulating palladium nanoparticles inside mesoporous MFI zeolite nanocrystals for shape-selective catalysis, *Angew. Chem., Int. Ed.*, 2016, **55**, 9178–9182.

23 L. C. Liu, U. Diaz, R. Arenal, G. Agostini, P. Concepcion and A. Corma, Generation of subnanometric platinum with high stability during transformation of a 2D zeolite into 3D, *Nat. Mater.*, 2017, **16**, 1272.

24 S. Goel, S. I. Zones and E. Iglesia, Encapsulation of metal clusters within MFI via interzeolite transformations and direct hydrothermal syntheses and catalytic consequences of their confinement, *J. Am. Chem. Soc.*, 2014, **136**, 15280–15290.

25 H. J. Cho, D. Kim, J. Li, D. Su and B. J. Xu, Zeolite-encapsulated Pt nanoparticles for tandem catalysis, *J. Am. Chem. Soc.*, 2018, **140**, 13514–13520.

26 W. Li, Y. H. Deng, Z. X. Wu, X. F. Qian, J. P. Yang, Y. Wang, D. Gu, F. Zhang, B. Tu and D. Y. Zhao, Hydrothermal etching assisted crystallization: A facile route to functional yolk-shell titanate microspheres with ultrathin nanosheets-assembled double shells, *J. Am. Chem. Soc.*, 2011, **133**, 15830–15833.

27 J. Du, J. Qi, D. Wang and Z. Y. Tang, Facile synthesis of Au@TiO_2 core-shell hollow spheres for dye-sensitized solar cells with remarkably improved efficiency, *Energy Environ. Sci.*, 2012, **5**, 6914–6918.

28 N. Zhang, S. Q. Liu, X. Z. Fu and Y. J. Xu, Synthesis of M@TiO_2 (M = Au, Pd, Pt) core-shell nanoconnposites with tunable photoreactivity, *J. Phys. Chem. C*, 2011, **115**, 9136–9145.

29 W. G. Tu, Y. Zhou, H. J. Li, P. Li and Z. G. Zou, Au@TiO_2 yolk-shell hollow spheres for plasmon-induced photocatalytic reduction of CO_2 to solar fuel via a local electromagnetic field, *Nanoscale*, 2015, **7**, 14232–14236.

30 P. Zhang and X. W. Lou, Design of heterostructured hollow photocatalysts for solar-to-chemical energy conversion, *Adv. Mater.*, 2019, **31**, 1900281.

31 N. Wang, Q. M. Sun, R. S. Bai, X. Li, G. Q. Guo and J. H. Yu, In situ confinement of ultrasmall Pd clusters within nanosized silicalite-1 zeolite for highly efficient catalysis of hydrogen generation, *J. Am. Chem. Soc.*, 2016, **138**, 7484–7487.

32 J. B. Cai, X. Q. Wu, S. X. Li, F. Y. Zheng, L. C. Zhu and Z. H. Lai, Synergistic effect of double-shelled and sandwiched TiO_2@Au@C hollow spheres with enhanced visible-light-driven photocatalytic activity, *ACS Appl. Mater. Interfaces*, 2015, **7**, 3764–3772.

33 Z. F. Jiang, W. Wei, D. J. Mao, C. Chen, Y. F. Shi, X. M. Lv and J. M. Xie, Silver-loaded nitrogen-doped yolk-shell mesoporous TiO_2 hollow microspheres with enhanced visible light photocatalytic activity, *Nanoscale*, 2015, **7**, 784–797.

34 M. G. Wang, J. Han, H. X. Xiong and R. Guo, Yolk@shell nanoarchitecture of Au@rGO/TiO_2 hybrids as powerful visible light photocatalysts, *Langmuir*, 2015, **31**, 6220–6228.

35 B. Cao, G. S. Li and H. X. Li, Hollow spherical RuO_2@TiO_2@Pt bifunctional photocatalyst for coupled H_2 production and pollutant degradation, *Appl. Catal., B*, 2016, **194**, 42–49.

36 Q. R. He, H. Sun, Y. X. Shang, Y. N. Tang, P. She, S. Zeng, K. L. Xu, G. L. Lu, S. Liang, S. Y. Yin and Z. N. Liu, Au@TiO_2 yolk-shell nanostructures for enhanced performance in both photoelectric and photocatalytic solar conversion, *Appl. Surf. Sci.*, 2018, **441**, 458–465.

37 K. E. deKrafft, C. Wang and W. B. Lin, Metal–organic framework templated synthesis of Fe_2O_3/TiO_2 nanocomposite for hydrogen production, *Adv. Mater.*, 2012, **24**, 2014–2018.

38 J. K. Zhang, Z. B. Yu, Z. Gao, H. B. Ge, S. C. Zhao, C. Q. Chen, S. Chen, X. L. Tong, M. H. Wang, Z. F. Zheng and Y. Qin, Porous TiO_2 nanotubes with spatially separated platinum and CoO_x cocatalysts produced by atomic layer deposition for photocatalytic hydrogen production, *Angew. Chem., Int. Ed.*, 2017, **56**, 816–820.

39 L. J. Gao, Y. G. Li, J. B. Ren, S. F. Wang, R. N. Wang, G. S. Fu and Y. Hu, Passivation of defect states in anatase TiO_2 hollow spheres with Mg doping: realizing efficient photocatalytic overall water splitting, *Appl. Catal., B*, 2017, **202**, 127–133.

40 J. Q. Yan, H. Wu, H. Chen, Y. X. Zhang, F. X. Zhang and S. F. Liu, Fabrication of TiO_2/C_3N_4 heterostructure for enhanced photocatalytic Z-scheme overall water splitting, *Appl. Catal., B*, 2016, **191**, 130–137.
41 X. Yu, J. Zhang, Z. H. Zhao, W. B. Guo, J. C. Qiu, X. N. Mou, A. X. Li, J. P. Claverie and H. Liu, NiO–TiO_2 p–n heterostructured nanocables bridged by zero-bandgap rGO for highly efficient photocatalytic water splitting, *Nano Energy*, 2015, **16**, 207–217.
42 P. F. Wang, S. H. Zhan, Y. G. Xia, S. L. Ma, Q. X. Zhou and Y. Li, The fundamental role and mechanism of reduced graphene oxide in rGO/Pt–TiO_2 nanocomposite for high-performance photocatalytic water splitting, *Appl. Catal., B*, 2017, **207**, 335–346.
43 K. F. Wu, H. M. Zhu, Z. Liu, W. Rodriguez-Cordoba and T. Q. Lian, Ultrafast charge separation and long-lived charge separated state in photocatalytic CdS–Pt nanorod heterostructures, *J. Am. Chem. Soc.*, 2012, **134**, 10337–10340.
44 K. F. Wu, H. M. Zhu and T. Q. Lian, Ultrafast exciton dynamics and light-driven H_2 evolution in colloidal semiconductor nanorods and Pt-tipped nanorods, *Acc. Chem. Res.*, 2015, **48**, 851–859.
45 J. B. Lee, S. Choi, J. Kim and Y. S. Nam, Plasmonically-assisted nanoarchitectures for solar water splitting: obstacles and breakthroughs, *Nano Today*, 2017, **16**, 61–81.
46 V. Subramanian, E. E. Wolf and P. V. Kamat, Catalysis with TiO_2/gold nanocomposites. effect of metal particle size on the Fermi level equilibration, *J. Am. Chem. Soc.*, 2004, **126**, 4943–4950.

